

## Experimental upper limit on the estimated thermal noise at low frequencies in a gravitational wave detector

A. Di Virgilio,<sup>1</sup> S. Bigotta,<sup>1</sup> L. Barsotti,<sup>1</sup> S. Braccini,<sup>1</sup> C. Bradaschia,<sup>1</sup> G. Cella,<sup>1</sup> V. Dattilo,<sup>2</sup> M. Del Prete,<sup>1</sup> I. Ferrante,<sup>1,3</sup> F. Fidecaro,<sup>1,3</sup> I. Fiori,<sup>1</sup> F. Frasconi,<sup>1</sup> A. Gennai,<sup>1</sup> A. Giazotto,<sup>1</sup> P. La Penna,<sup>2</sup> G. Losurdo,<sup>4</sup> E. Majorana,<sup>5</sup> M. Mantovani,<sup>6</sup> F. Paoletti,<sup>1,2</sup> R. Passaquieti,<sup>1,3</sup> D. Passuello,<sup>1</sup> F. Piergiovanni,<sup>7</sup> A. Porzio,<sup>8</sup> P. Puppo,<sup>5</sup> F. Raffaelli,<sup>1</sup> P. Rapagnani,<sup>5,9</sup> F. Ricci,<sup>5,9</sup> S. Solimeno,<sup>8,10,11</sup> G. Vajente,<sup>1,12</sup> and F. Vetrano<sup>4,7</sup>

<sup>1</sup>*INFN, Sezione di Pisa, Italy*

<sup>2</sup>*European Gravitational Observatory, Cascina (Pi), Italy*

<sup>3</sup>*Università di Pisa, Italy*

<sup>4</sup>*INFN Sezione di Firenze, Italy*

<sup>5</sup>*INFN Sezione di Roma, Italy*

<sup>6</sup>*Università di Siena, Italy*

<sup>7</sup>*Università di Urbino, Italy*

<sup>8</sup>*Coherentia, CNR-INFN, and CNISM Unità di Napoli, Italy*

<sup>9</sup>*Università di Roma La Sapienza, Italy*

<sup>10</sup>*INFN Sezione di Napoli, Italy*

<sup>11</sup>*Università di Napoli Federico II, Italy*

<sup>12</sup>*Scuola Normale Superiore, Pisa, Italy*

(Received 23 December 2006; published 21 December 2007)

The mirror relative motion of a suspended Fabry-Perot cavity is studied in the frequency range 3–100 Hz. The experimental measurements presented in this paper have been performed at the Low Frequency Facility, a high finesse optical cavity 1 cm long suspended to a mechanical seismic isolation system like the one of the VIRGO gravitational wave antenna. Because of the radiation pressure between the two mirrors of the cavity, the dynamic behavior of the system is characterized by the optical spring stiffness. In the frequency region above 3 Hz, where seismic noise contamination is negligible, the mirror displacement noise is stationary and its statistical distribution is Gaussian. Using a simplified mechanical model of the suspended system and applying the fluctuation dissipation theorem, we show that the measured power spectrum is reproduced in the frequency region 3–90 Hz. Since the contribution coming from different sources of the system to the total noise budget turns out to be negligible, we conclude that the relative displacement power spectrum of this opto-mechanical system is compatible with a system at thermal equilibrium within its environment. In the region 3–10 Hz this measurement gives so far the best upper limit for the thermal noise of the suspension for a gravitational wave interferometer.

DOI: [10.1103/PhysRevD.76.122004](https://doi.org/10.1103/PhysRevD.76.122004)

PACS numbers: 04.80.Nn, 07.60.Ly, 42.50.Lc, 42.65.Sf

### I. INTRODUCTION

The large interferometers for gravitational waves detection and study are close to full operation. The LIGO detectors have been operated at the design sensitivity all over their detection bandwidth while the VIRGO interferometer is approaching the goal sensitivity, improving its performance also in the low frequency region where several gravitational wave signals are expected [1]. Even if these detectors are based on the same working principle, the VIRGO interferometer has been conceived with a mechanical suspension, the superattenuator (SA), to suppress the seismic noise transmission to the optical components by more than 10 orders of magnitude starting from about 3 Hz [2,3]. In the low frequency region thermal fluctuations of mechanical systems are considered the most relevant limitation of ground based interferometers. Their statistical behavior is well described by the fluctuation dissipation theorem, connecting the system response to an external disturbance to the inner fluctuations of the system itself, when no disturbances are present. Such a

response is characterized by the mechanical admittance (or impedance) of the structure [4–6].

The test masses for gravitational wave interferometers are complex mechanical systems where contributions to the thermal noise come from different elements of the structure: the suspension wires of the mirror, the mirror bulk, and the mirror coating, which is considered one of most severe thermal-noise sources for the present and near future detectors, just to mention a few of them. Measurements devoted to the evaluation of different dissipation mechanisms and of the parameters describing them are often performed on resonance. Just a few experimental apparatus have been conceived to measure the thermal-noise spectrum out of resonance and in the frequency region above 100 Hz [7–10]; more recently the CLIO cryogenic interferometer is investigating the lower frequency region [11]. Our apparatus looks at the displacement power spectrum in the 10 Hz frequency range, far from resonances. The Low Frequency Facility's (LFF's) main purpose is the relative displacement measurement of two mirrors forming a high finesse Fabry-Perot cavity

suspended from a seismic isolation system and the study of the thermal-noise spectrum in the region starting from 10 Hz [12]. The experimental apparatus is installed at the INFN Pisa laboratory, where a superattenuator, very similar to those ones installed along the two arms of the VIRGO interferometer, has been mounted. Particular care has been devoted to the experiment design and its final installation keeping the apparatus as similar as possible to the VIRGO suspension chain. The main differences between the two apparatus (VIRGO and LFF) is the presence of the optical spring and one more mirror (the AX mirror) which will be described in the next paragraph. Moreover, since seismic noise reduction to the payload level is very large, the LFF can be considered as an independent benchmark of the VIRGO suspension behavior in the low frequency region. Recently, data collected with the LFF has shown the presence of an optical spring due to the radiation pressure noise of the system [13]. Within the frequency band 3–90 Hz this thermal-noise dominated setup is unique as well as the presence of the optical spring acting between the two mirrors of the cavity. The frequency region 3–10 Hz is very interesting especially for the study of signals emitted by pulsars [14], and will not be covered by space antennas as Lisa; in this frequency region the big antennas' response is dominated by noise coming from the servo loops, and the LFF apparatus gives so far the best upper limit for the suspension thermal noise.

The first section of this paper shortly describes the experimental apparatus. An introduction to a simplified mechanical model reproducing the experimental measurements is presented in the second section; the model is necessary to extract information for the VIRGO apparatus. Hence the third section is focused on the evaluation of the main noise coming from external sources of the system. In the fourth section a general overview on the measured spectra is given, paying particular attention to the main characteristics of the thermal-noise driven mechanisms, and the dissipation coefficients found fitting the data with the model are discussed. In the subsection the thermal-noise upper limit for the Virgo suspension and the nonlinearities and up-conversions are treated. In the last section, before the conclusions, the results are discussed.

## II. THE EXPERIMENTAL SETUP AND THE DATA ACQUISITION CHAIN

The last stage of the experimental apparatus is sketched in Fig. 1 while a more detailed description can be found in Ref. [12]. The reflectivity, transmission, and loss ( $R_i$ ,  $T_i$ ,  $A_i$  with  $i = 1, 2$  respectively) of the two mirrors used in our setup are given in Table I together with the nominal cavity finesse  $\mathcal{F}$  and the laser input power  $P_{\text{in}}$ . The reference cavity (RFC) and the suspended mirrors (represented within a gray box in Fig. 1) are installed within two vacuum tanks.

TABLE I. Optical parameters of the cavity.

$R_1$	0.9991
$R_2$	0.9999
$A_1$ and $A_2$	0.00001
$T_1$	0.0009
$\mathcal{F}$	6300
$P_{\text{in}}$	200 mW

The cavity finesse  $\mathcal{F}$ , evaluated from the transmission profile of the uncontrolled system (no feedback loop active), is about  $5500 \pm 1500$ . The static radiation pressure force is about  $5 \mu\text{N}$ . The suspension system adopted to isolate the high finesse 1 cm long Fabry-Perot cavity from seismic noise is a single SA conceived for the VIRGO interferometer test masses [4]. The curved mirror, having a diameter of 25 mm, is embedded in a large steel cylinder forming the mirror holder. It plays the role of the VIRGO test mass (VM). The flat mirror of the cavity (AX, auxiliary mirror) is hung, by means of an independent three-stage suspension, to the last mechanical seismic filter of the chain called Filter7. Along this branch of the chain an intermediate mass ( $m_d$ ) has been included as well as a small clamp of the AX suspension wire ( $m_t$ ). The control of the longitudinal motion is done by acting only on the VM mirror using two coil-magnet pairs. This actuation technique is identical to that one implemented in the VIRGO interferometer [2,15,16] where the coils are screwed on the reference mass (RM) and the magnets are glued on the back side of the mirror. Figure 1 shows the cavity, the input beam, the longitudinal control loop scheme, and the acquired signals. The laser beam, phase modulated at 17 MHz and independently frequency stabilized on a 15 cm rigid reference cavity made of ULE (low expansion glass, supplied by Corning) material, is injected into the Fabry-Perot cavity. The reflected power, deviated by the polarizer, is detected by a photodiode and demodulated by the mixer. We applied the Pound-Drever-Hall scheme (P-D-H) similar to that one used for the VIRGO prestabilization circuit, which should provide a laser frequency stabilization of the order of  $\sim 1 \text{ mHz}/\sqrt{\text{Hz}}$ . [17]. The linear zone of the readout signal is about  $10^{-10} \text{ m}$ . The feedback control loop is based on a digital signal processor (DSP) developed for the VIRGO suspension control system. The cavity signal is amplified and then sent to a 16 bit analog-to-digital converter (ADC) board while the DSP performs the signal filtering to control the stability of the longitudinal loop. The filtered signal is sent to four digital-to-analog converter (DAC) (20 bit) channels and then to the four coil drivers. Mixer output, coil voltage (both signals filtered by an antialiasing filter at 3.4 kHz), and the current flowing in the coil are relevant signals acquired during the measurements through a LABVIEW program at an acquisition rate of 400 Hz. They are labeled in Fig. 1 as ERROR, COIL2, and PROBE, respectively. The LFF values of the

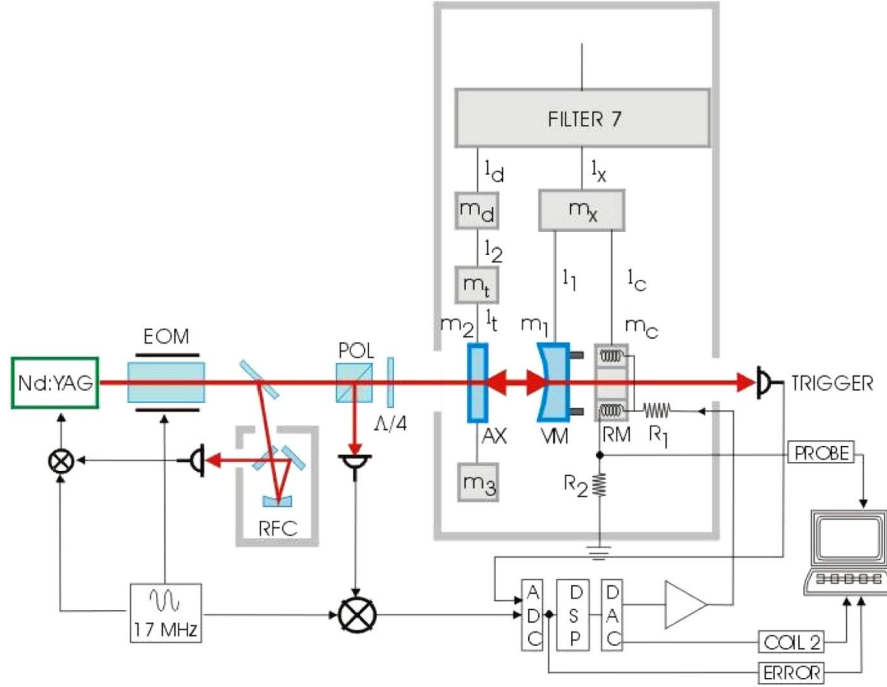


FIG. 1 (color online). Sketch of the experimental setup starting from Filter7; gray boxes put in evidence all the components within the vacuum tanks. The optical layout and the data acquisition chain are shown.

TABLE II. Mechanical characteristics of the LFF system.

Masses	kg	Wires	mm
$m_d$	71.72	$l_d$	1100
$m_t$	0.08	$l_t$	250
$m_2$	0.296	$l_2$	500
$m_3$	2.5	$l_3$	300
$m_x$	80	$l_x$	1130
$m_1$	27.61	$l_1$	700
$m_c$	64.14	$l_c$	500

TABLE III. Electro-optical parameters of the LFF system.

E.M. actuator coupling $\alpha$	3 mN/A
Optical gain $G_{opt}$	$1.56 \times 10^{10}$ V/m
Feedback loop gain range	$10^5 - 10^6$
Unity gain frequency	150 Hz
RMS displacement (open loop)	$> 10^{-6}$ m
RMS displacement (closed loop)	$< 10^{-11}$ m

mechanical and electro-optical parameters are summarized in Tables II and III.

### III. MECHANICAL MODEL AND EXPERIMENTAL MEASUREMENTS

The thermal noise of a linear mechanical system is computed according to the fluctuation dissipation theorem [4,5,18]. The theorem states that the thermal-noise spec-

trum of a mechanical oscillator in thermal equilibrium with its bath is given by

$$x^2(\omega) = \frac{4k_B T}{\omega^2} \text{Re}[Y(\omega)] \tag{1}$$

where  $k_B$  is the Boltzmann's constant,  $T$  the bath temperature,  $\omega = 2\pi\nu$ , with  $\nu$  the frequency, and  $Y(\omega)$  the system admittance defined as

$$Y(\omega) = \frac{v(\omega)}{F(\omega)} \tag{2}$$

where  $F(\omega)$  is the amplitude of the external force responsible of the system motion with a velocity of amplitude  $v(\omega)$ . In order to predict the noise behavior of the LFF payload, the oscillator system has been modeled assuming massless wires and rigid bodies. Although the superattenuator chain adopted to isolate the optical components from seismic noise is a complex system, the model is limited to the study of the dynamical elements of the payload, i.e., the coupled oscillators forming the two branches hung to Filter7 (see Fig. 1). Each branch includes one mirror of the optical cavity: the first one (AX) is made of four masses suspended in series while the second one (VM) is composed by a simple pendulum from which two elements are attached in parallel. The system of the equations of motion for the mechanical elements sketched in Fig. 1 includes four equations describing the AX side motion, and three others the VM side. Moreover, since

the suspended flat mirror has rotational oscillation modes below 10 Hz, we included also coupling terms and equations related to the rotational degrees of freedom of the AX mirror. The oscillation modes of the suspension wires of 300  $\mu\text{m}$  diameter and the internal oscillation modes of the mirrors can be derived only if we model the apparatus as a continuous system. However the family of transversal modes of the wires (violin modes) starts around 100 Hz and the internal modes of the mirror are at even higher frequency. Since we are modeling just the low frequency part of the spectrum, the hypothesis of massless wires and rigid body is robust. Details of the model are reported in the appendix.

We included in the equations of motion the loss terms. We treated the two cases: the viscous damping with a term  $\gamma$  times the velocity, and the structural damping by a complex spring constant  $k(1 + i\phi)$  where  $\phi$  is the loss angle usually assumed constant with frequency and smaller than  $10^{-4}$  [19,20]. At low frequency this assumption is controversial [21], so that in principle we cannot exclude that a structural damping can mimic the typical spectral behavior of a viscous oscillator, with the relation  $\phi = \omega \gamma/k$ . The dissipation mechanisms have been introduced for 2 degrees of freedom: the longitudinal and rotational motion of the mirror. Since the AX pendulum has a mass 100 times smaller than that one of the VM mirror, we expect that the main contribution to the system thermal noise is associated to the AX mirror dissipation. Thus, our measurement can be used just to set a thermal-noise upper limit for the VIRGO-like mirror. The model includes also the feedback loop and the optical spring effect. The feedback loop takes into account the coil driver impedance and the filter function computed by the DSP board (see Fig. 1)

on the base of the mechanical transfer function of the system represented as a combination of zeros and poles.

On the base of these coupled equations we set up a simulation code using the MATHEMATICA software package. The software simulation is flexible enough to provide the response of the system when extra noise is injected in different points of the LFF scheme (see Fig. 2).

In particular, the thermal-noise contribution within the mirror relative displacement  $x$  measurement (the ERROR signal of the feedback longitudinal control loop in Fig. 2) has been evaluated as follows:

- (i) in the open loop configuration the mechanical impedance has been estimated applying forces of the same amplitude and opposite direction to both mirrors of the cavity;
- (ii) on the base of the derived mechanical impedance and by applying the fluctuation dissipation theorem the spectrum of stochastic forces has been evaluated;
- (iii) in the closed loop configuration (to be compared with the experimental data), we computed the mechanical response of the system by applying to the mirrors thermal stochastic forces previously derived. Experimental data have been compared with the model prediction using as free parameters of the fit, the dissipation coefficients and the optical spring stiffness.

Figure 3 shows thermal-noise spectra in different working conditions: open loop with and without optical spring, and in closed loop condition with optical spring; it clearly shows that the optical spring strongly affects the power spectrum, reducing the motion at low frequency and increasing it around the optical spring resonance.

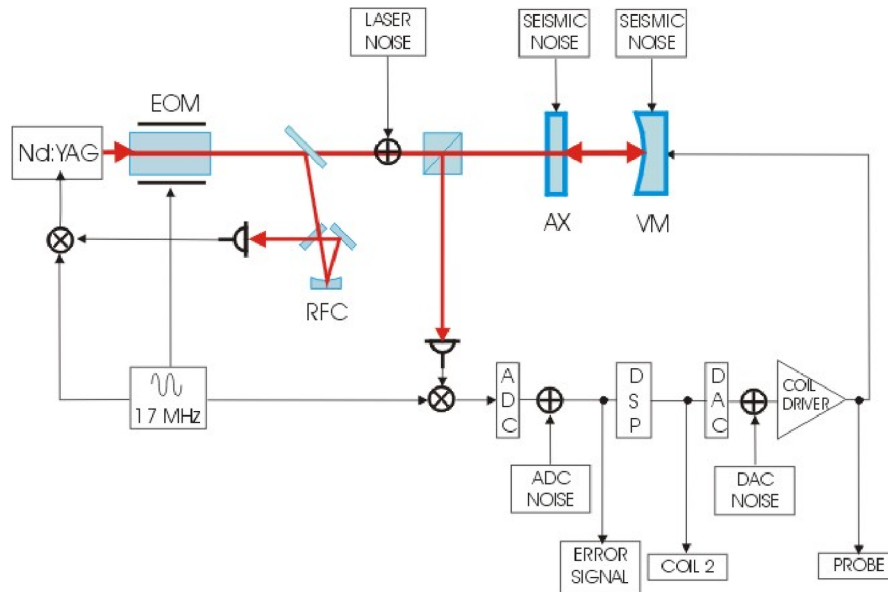


FIG. 2 (color online). Scheme of the control loop, which includes the main noise sources.

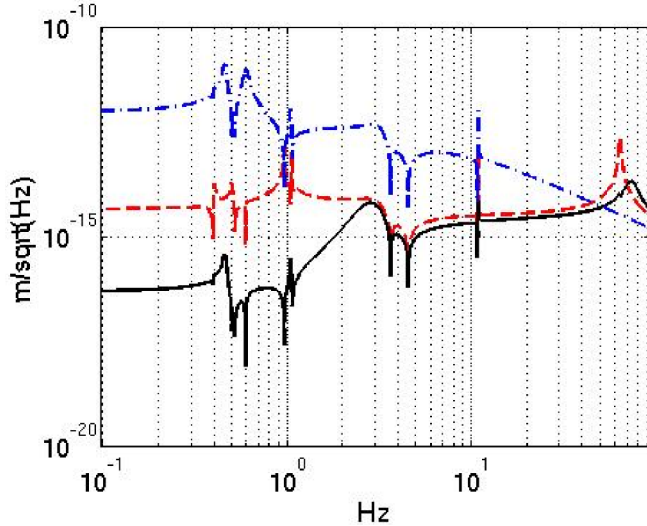


FIG. 3 (color online). Thermal-noise power spectrum in the three cases: open feedback loop without optical spring (dot-dashed line), open feedback loop with optical spring (dashed line), closed feedback loop with optical spring (continuous line).

#### IV. EXTRA NOISE SOURCES

In Fig. 4 the power spectrum of the two mirrors' relative motion suspended to the SA chain is shown. This plot has been obtained analyzing a collected data stretch 1 h long.

A typical structure of the SA chain excited by the seismic noise is visible below 3 Hz while at higher frequency a few peaks with high mechanical quality factor ( $Q$ ) are present. In particular, the broad peak coming from the optical spring at about 90 Hz is well visible. In the frequency region above 3 Hz, we tried to identify as many as possible noise sources of our experimental setup. First of

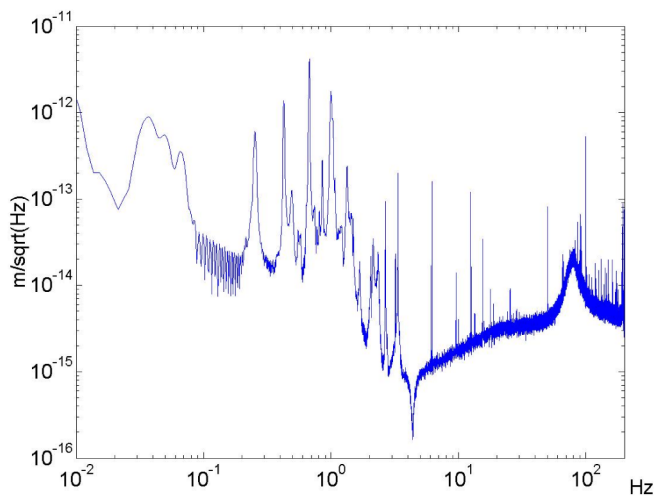


FIG. 4 (color online). Typical power spectrum of the mirror relative motions in the suspended cavity. The measurement has been obtained with the feedback loop active.

all we notice that the noise spectrum is characterized by several peaks originated by a few different mechanisms like the mechanical vibration of the vacuum vessel, fluctuation of the input laser beam (whose optical path is in air), or the environmental electromagnetic pollution. As a preliminary step of the data analysis, we checked that the nonstationary behavior of some of these peaks does not influence the noise floor. For this purpose we compared consecutive time slots of a single data acquisition and we verified that while the amplitude peak enhanced, the noise floor remained constant [12].

Thus, all the noise sources due to a nonstationary mechanism have been ruled out. In Fig. 2 we located in the scheme the various extra noise sources.

Seismic noise propagates to the payload through the suspension system only. The residual rms motion of the mirror is several microns in the open loop configuration and less than  $10^{-11}$  m when the feedback loop is on. The measurement above 3 Hz is incompatible with the seismic noise, for several reasons: the seismic noise is nonstationary and the spectral behavior should be very different from the measured one. Moreover, some runs have recorded the data from the cavity and from accelerometers located nearby, inside the vacuum tank of the suspension. Above 3 Hz the coherence between the cavity error signal and the seismic motion is below 1%. A detailed analysis of the seismic noise contamination in the case of the mirror suspended by the superattenuator can be found elsewhere [22]. Here we recall that the contamination of seismic noise at 10 Hz is below  $10^{-15}$  m/ $\sqrt{\text{Hz}}$  for the VIRGO interferometer test masses. Other noise sources are associated to different devices: the laser (frequency and amplitude jitters), the mixer, the photodiode, the coil drivers, as well as the ADC and DAC boards. In the following we analyze their contributions to the LFF output spectrum.

- (i) The noise due to the DAC board and the coil drivers, indeed, results to be incompatible with the measured spectrum. A power spectrum similar to that one measured during our data taking corresponds to a DAC noise value of  $2 \times 10^{-4}$  V/ $\sqrt{\text{Hz}}$ , a factor  $10^3$  higher than that one measured on bench. In fact, the coherence study between the signal acquired at the output of the DAC board (COIL2 label in Fig. 2) and the signal acquired after the coil driver (PROBE label in Fig. 2) representing the current flowing in the coil) is higher than 95% above 10 Hz. We conclude that the DAC noise contribution to the total noise budget is negligible.
- (ii) When we consider in the model the combined effect of different noise sources (laser, mixer, photodiode, and ADC board), we conclude that a white noise would not reproduce the collected data in the frequency band 3–100 Hz. In Fig. 5 the ratio between the noise injected within the system and the ERROR

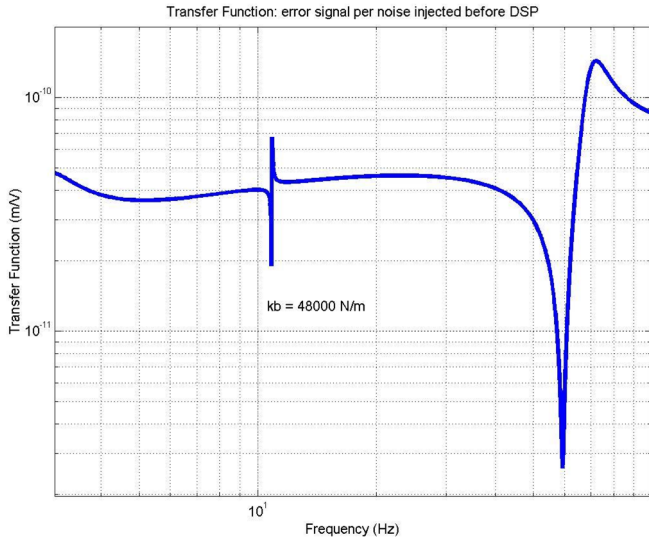


FIG. 5 (color online). PROBE output versus frequency computed in the model by injecting white noise before the DSP.

signal (see the relative label in Fig. 2) is plotted on this frequency range. In particular, the peak around 80 Hz is compatible with a spectral density noise of the source  $\sim 1.5 \times 10^{-3} \text{ V}/\sqrt{\text{Hz}}$ . However, the larger source of noise originates in the ADC board; we have measured its spectral density as  $2.4 \times 10^{-6} \text{ V}/\sqrt{\text{Hz}}$  at a sampling frequency of 10 kHz. We conclude that also this noise contribution is negligible.

- (iii) The frequency jitters of the Nd:YAG laser source could be the dominant source of noise. However, the measured power spectrum around the optical spring resonance (around 80 Hz) is compatible with a frequency jitter of  $\sim 350 \text{ Hz}/\sqrt{\text{Hz}}$ , just a factor 5 below the measured free running laser frequency jitter. However, during data taking the laser source is frequency stabilized at the level of a few  $\text{mHz}/\sqrt{\text{Hz}}$ , so that it results that this noise source contribution is at least  $10^6$  times lower than the total noise spectrum.

The sum of the frequency and amplitude jitter of the laser and the photodiode noise have been measured independently. The P-D-H reflected signal has been recorded at a sampling rate of 40 kHz with the optical cavity out of lock. Studying the linear region of the P-D-H signal, we can evaluate the sum of the above mentioned noises. The collected data have been fitted with a polynomial curve up to the ninth order, then the statistical distribution of the residuals was studied. The standard deviation of this last distribution is a good estimator of the noise affecting the system [23]. The obtained value  $2 \times 10^{-4} \text{ V}$  reported on Fig. 6 is not compatible with a power spectral density of  $1.5 \times 10^{-4} \text{ V}/\sqrt{\text{Hz}}$ .

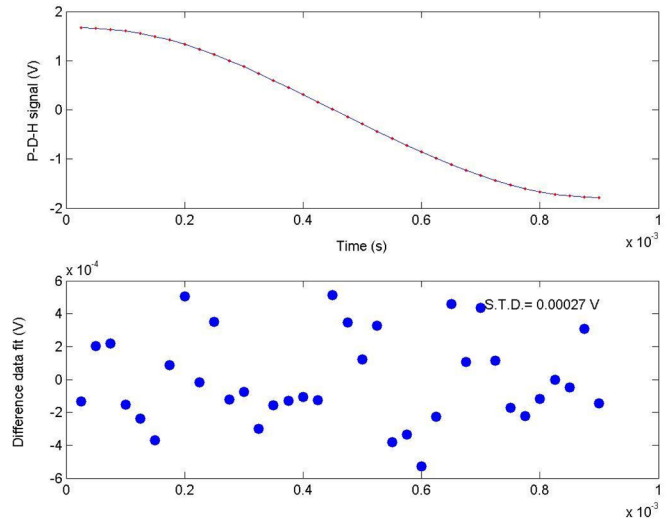


FIG. 6 (color online). Top: P-D-H signal around the resonance, feedback not active; over-imposed is the polynomial fit of the recorded points up to order 9. Bottom: difference measured points polynomial fit, which is a good measure of the noise coming from the laser, frequency, and amplitude noise.

### Thermal-noise upper limits for the Virgo mirrors and up-conversion.

Thermal-noise upper limits for the open loop motion of the VM branch can be evaluated in the low frequency region with the help of the mechanical model and using the fitted parameters. The stochastic forces are evaluated from the data, and then applied to the Virgo mirror suspension only, considered isolated, without the optical spring which couples the two mirrors. Figure 7 shows the upper limit of the thermal noise of the Virgo interferometer

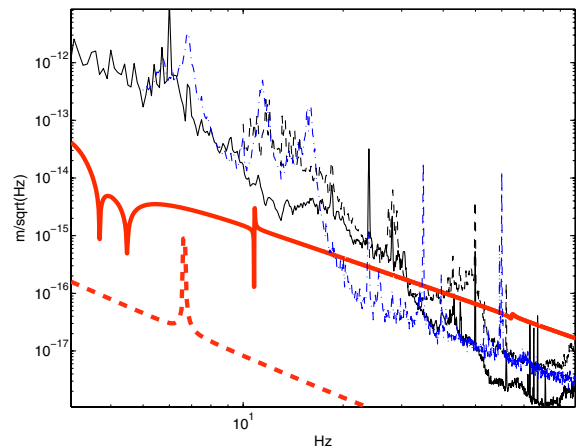


FIG. 7 (color online). Thick continuous line: Upper limit of thermal-noise displacement noise of the VIRGO mirrors. Thick dotted line: expected thermal noise for the VIRGO interferometer. Thin dotted line: VIRGO sensitivity in WSR6, 1st–4th December 2006. Thin continuous line: VIRGO sensitivity in WSR10, 9th–12th March 2007. Thin dashed-dotted line: CLIO sensitivity as extracted from [24].

test masses, which is compared with the noise evaluated by the Virgo interferometer [14]; the Ligo and Geo600 data are not shown since they have not been designed for such low frequencies. The CIO Japanese interferometer, a cryogenic facility, located in the Kamioka mine is pushing hard to have good sensitivity at low frequency [25,26]. One of the main problems of the low frequency region is done by the up-conversions: the large low frequency motion generates noise at higher frequency by nonlinear couplings, which could be due as well to the mechanical apparatus or the electronics. The data analyzed are Gaussian, they have passed MATLAB tests, bi-spectra has been studied as well, linearities are not present, and no evidence of up-conversion have been found in this set of data. The typical relative open loop motion of the two mirrors was 5–10  $\mu\text{m}$ , and it is possible to say that up-conversions of the low frequency motion (several microns) are not present in the interval 3–100 Hz).

## V. RESULTS OF THE FIT AND DISCUSSION

We collected data in several different working conditions but with similar control loop gain. The test performed confirms the compatibility of the data with the thermal-noise prediction. As mentioned in a previous paragraph the most important signal used in our analysis is that related to the cavity detuning (closed loop error signal) obtained by reconstructing the signal output of the DSP (COIL2 in Fig. 1). This signal is acquired after a two poles Butterworth filter, which selects the frequency range 10–200 Hz. The region of the spectrum below 3 Hz is dominated by the seismic noise, and it has been cut off by another high pass filter applied to the data. Using the Horde software routine of the MATLAB package, we checked that the data follows the Gaussian statistical distribution, and the time-frequency spectrograms show that it is stationary. According to Ref. [4] an independent check of the stationary data for a thermal-noise dominated system can be evaluated averaging the product between the speed and the acceleration of the observed system ( $\langle v_x \cdot a_x \rangle$ ;  $v_x$  and  $a_x$  are the speed and the acceleration). This parameter should vanish if the system is thermal-noise dominated. Figure 8 shows the distribution of the mentioned parameter (the average of the product between the speed and the acceleration of the system) averaged on increasing time interval and for frequencies below 100 Hz. The speed and the acceleration have been obtained by differentiating the displacement measurements. As stated by the Boltzmann's law, the distribution of the speed ( $v_x$ ) for an oscillator excited by the thermal noise is

$$f(v_x) = \left(\frac{m}{2k_b T}\right) \left(\frac{1}{2}\right) \times e^{-(mv_x^2/2k_b T)}, \quad (3)$$

where  $m$  is the oscillator mass,  $k_b$  is the Boltzmann's constant, and  $T$  the absolute temperature. Moreover, the variance  $\sigma$  of the distribution  $f(v_x)$  for a free oscillating

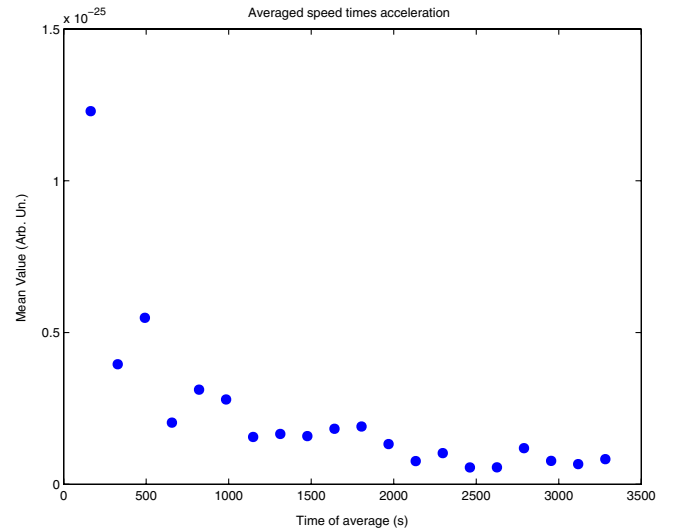


FIG. 8 (color online). Speed times acceleration averaged over time intervals of increasing length.

system (not feedback controlled) is defined by the mechanical parameters. Our measurements have been performed with an active feedback loop which does not influence the distribution of the data, but it changes the absolute value of the variance itself. In principle the variance  $\sigma$ , for a closed loop case, could be reconstructed integrating the expected power spectrum all over the frequency band. The comparison between the measured spectrum and the predicted one is the most reliable method to prove that the data are thermal-noise dominated. Thus, we checked that the energy associated with the mirror AX, integrating the power spectrum between 3 and 100 Hz, is below  $k \times T/2$  ( $T \approx 298$  K).

Kubo [4] states that for a system at the thermal equilibrium the admittance  $Y$  can be evaluated by the Fourier transform integrated from zero to infinity of the autocorrelation function of the speed. From the knowledge of  $Y$  it is possible to reconstruct the power spectrum from the fluctuation dissipation theorem. Let  $x_F$  be the displacement filtered by the feedback loops and by the filters of the acquisition system. The following relation held for the power spectrum of  $x_F$ :

$$S_{x_F x_F} = \frac{2}{\omega^2} \Re \left[ \int_0^\infty \left\langle \frac{dx_F(t+\tau)}{dt} \frac{dx_F(t)}{dt} \right\rangle e^{i\omega t} dt \right]. \quad (4)$$

In Fig. 9 the  $S_{x_F x_F}$  is evaluated both directly from the data and applying the above equation. The agreement is good, in particular, in the region of the optical spring resonance and at higher frequencies. At lower frequency the stretch of data is too short to be used for deriving a significant estimation of the power spectrum on the basis of the formula reported above. The good agreement shown is not sufficient to demonstrate that our measurements are thermal-noise dominated. It represents just an efficient

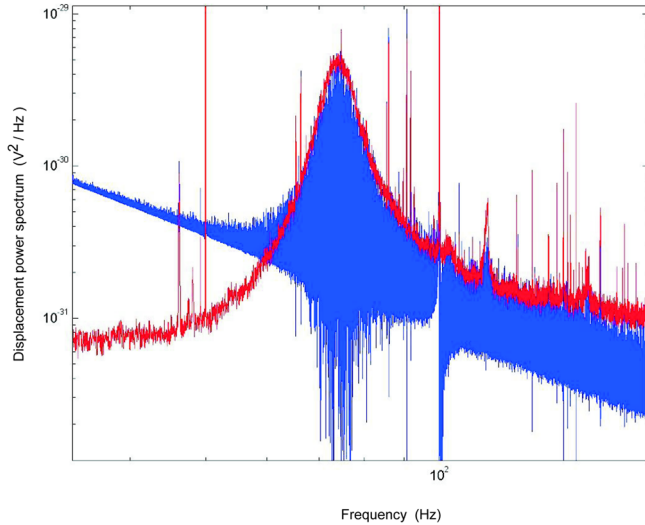


FIG. 9 (color online). Measured power spectrum compared with the power spectrum reconstructed by evaluating the admittance from the speed autocorrelation function and applying the fluctuation dissipation theorem; see Eq. (4).

cross-check performed using uncalibrated raw data. To evaluate in a more precise way the thermal-noise contribution to the data, we used our model to best fit the data. First of all, we derived the dissipation coefficient  $\gamma_l = 5.8$  1/s, associated to the longitudinal motion of AX, by fitting the data selected around the optical spring resonance 65–80 Hz, while the other  $\gamma_\theta = 6.5$  1/s is found by fitting the data in the interval 3.5–6 Hz, where there is the anti-resonance. In Fig. 10 we show the measured spectrum and the thermal-noise contribution estimated by best fitting the data with the model for an optical gain  $G_{\text{opt}} = 1.56 \times 10^{10}$  V/m and  $k_b = 56\,000$  N/m. Similar results have been obtained by analyzing the data of independent runs. Since the pressure inside the vacuum tank was lower than  $10^{-4}$  mbar, we checked [27] that the estimated dissipation coefficients are incompatible with losses due to the residual gas. It has been also checked that the present measurement is not compatible with a loss angle  $\phi$  constant in frequency, but it agrees with viscous damping or equivalently a loss angle frequency depending [21]. As it is shown in Fig. 10, the result of the fit and the data well agree below 90 Hz, at higher frequency the higher order modes are relevant, and the model cannot reproduce the data. In fact, the power spectrum of the collected data is limited below 200 Hz and it is impossible to further constrain the model by adding higher order modes, since the high frequency resonance cannot be identified. We checked just with the model that higher internal modes of the mirrors and violin modes of the wires change the slope of the power spectrum above 100 Hz and increase the level at lower frequency.

We notice that the dissipation coefficients are about 10 times larger than expected in a gravitational wave experiment. However, if the losses are due to the clamps of the

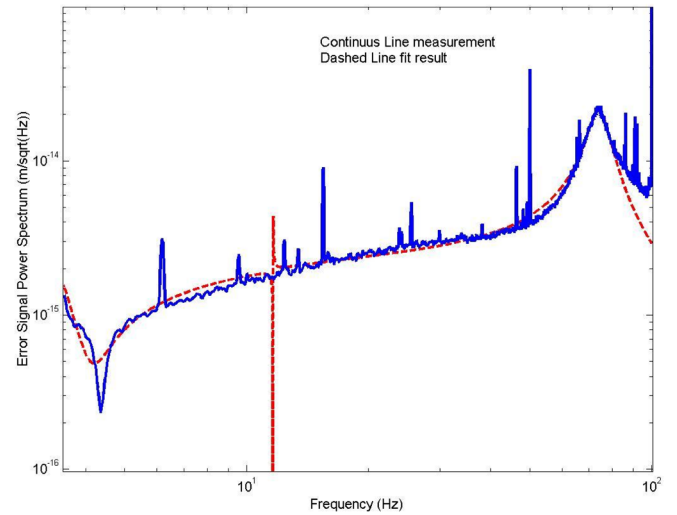


FIG. 10 (color online). Measured power spectrum, 10 mHz frequency resolution, compared with the thermal -noise estimated by the model, assuming an optical gain  $1.56 \times 10^{10}$  V/m,  $k_b = 55\,000$  N/m, and the typical working conditions of the present set of runs; the losses, two parameters constant in frequency, are associated to the AM longitudinal and rotational degree of freedom; their fitted values are  $5.8$  1/s for the longitudinal and  $6.5$  1/s for the rotational.

suspension, the present result should be considered as a warning for the present large interferometric antennas. However the large values of dissipation factor resulting from the fit can be biased for the reasons discussed in the following.

- (i) The LFF apparatus is not as performing as VIRGO from the point of view of the losses due by mechanical dissipation. In particular three wire loops are attached to the AX mirror and the wire diameter is rather large ( $300$   $\mu\text{m}$ ). Moreover the two wire loops holding the mirror are attached to a motor used to align horizontally the cavity. Because of the fact that the difference in length of the two wire loops, set up only 3 mm apart, was causing a large vertical misalignment, it has been necessary to change the length of one of the two wire loops by using a clamp, which is attached directly to the wires of one of the two loops. This clamp consists of two pieces and a screw, which bends the AX, changing the distance between the two pieces and the effective length of one of the two wire loops mirror.
- (ii) The model overestimates the losses for two reasons: in the model the losses are associated to the AX mirror motion only, and the higher order mechanical modes of the system are not taken into account. Indeed, we checked that in principle the higher order mode tail at low frequency can contribute in decreasing the dissipation coefficients.
- (iii) The values of the two  $\gamma$  coefficients resulting from the data fit depend also on the absolute calibration: in

particular, they decrease when the optical gain is increased. For example, assuming a optical gain  $6 \times 10^{10}$  V/m, the fit gives  $\gamma_l = 0.13$  1/s and  $\gamma_\theta = 1.06$  1/s. The calibration of the LFF apparatus so far relies on measurements taken when the cavity feedback is off (open loop condition). The actuator system is calibrated applying a slowly increasing voltage to the coil drivers and counting the number of free spectral ranges transmitted by the cavity. In practice, the optical readout is calibrated by looking at the Pound-Drever-Hall signal; the two sidebands 34 MHz apart set the scale for the absolute calibration. In order to improve the calibration accuracy of the measurement, it would be necessary to have an independent system pushing the mirror a known amount during the data taking.

## VI. CONCLUSIONS

A 1 cm Fabry-Perot cavity is suspended using a super attenuator chain equal to the ones used for the VIRGO antenna. This cavity has been locked for several hours, and data analyzed offline. The output signal exhibits a statistical behavior and a displacement power spectrum compatible with a system at its thermal equilibrium. For the first time we have been able to measure, out of the mechanical resonances, the thermal noise of suspended mirrors in the range 3–100 Hz which includes the optical spring resonance. The data have been compared with a prediction of a simplified opto-mechanical model. On the base of it we evaluated the relative contribution of different noise sources of the system and, in particular, that one of the thermal noise computed applying the fluctuation dissipation theorem. We concluded that the measured power spectrum is not dominated by external noise sources. The spectrum is compatible with the thermal noise of the suspended mirror dominated by viscous dissipation coefficients  $\gamma_l = 5.8$  1/s and  $\gamma_\theta = 6.5$  1/s associated to the AX mirror. Upper limits for pendulum thermal noise are evaluated for the Virgo suspension in the low frequency region, showing that future antennas could extend the detection bandwidth down to a few Hz; up-conversion of the low frequency motions are not evident in the data. So far this is the best upper limit in the frequency region 3–10 Hz.

## ACKNOWLEDGMENTS

We would like to gratefully acknowledge F. Marchesoni for stimulating discussions. We would like to thank all the technicians of the Pisa-INFN sections, who have contributed to the construction of the LFF experiment: R. Cosci, C. Magazzú, A. Di Sacco, A. Del Colletto, F. Mariani, and M. Iacoponi. We thank M. Perciballi and M. Iannone of Rome, P. Dominici of Urbino, and S. Di Franco of Florence. Special thanks goes to M. Ciardelli, R. Macchia, F. Nenci, and A. Pasqualetti currently at EGO.

## APPENDIX: MODEL EQUATIONS

We report here the equations of motion of the simplified LFF model just in the case of viscous damping terms added to the AX mirror. We refer to the symbols reported in Fig. 1. The first group of five equations are associated to the AX suspension; four of them are related to the longitudinal degree of freedom of the masses and the fifth one to the rotation of the AX mirror around the vertical axis.  $F_{x_d}$ ,  $F_{x_t}$ ,  $F_{x_2}$ , and  $F_{x_3}$  are the forces applied to the masses  $m_d$ ,  $m_t$ ,  $m_2$ , and  $m_3$ , while  $M$  is the torque applied to the AX mirror. The other three equations are related to the mass longitudinal motion of the branch which includes the VM mirror.  $F_{VM_x}$ ,  $F_{VM_c}$ , and  $F_{VM_1}$  are the forces applied to the mass  $m_x$ ,  $m_c$ , and  $m_1$ , respectively.

$$F_{x_t} = -m_d \omega^2 x_d + \frac{(m_d + m_2 + m_3 + m_t)(x_d - ns_d)}{l_d} + \frac{g(m_t + m_2 + m_3)}{l_2}, \quad (\text{A1})$$

$$F_{x_t} = -m_t \omega^2 x_t - \frac{g(m_t + m_2 + m_3)(x_d - x_t)}{l_2} + \frac{g(x_t - x_2)(m_2 + m_3)}{l_t}, \quad (\text{A2})$$

$$F_{x_2} = -m_2 \omega^2 x_2 - \frac{g(m_2 + m_3)(x_2 - x_t)}{l_t} - \frac{g(x_3 - x_2)(m_3)}{l_3} + k_{\text{opt}}(x_2 + x_b - \theta l_r) + i \cdot \omega \gamma_l^1 x_2, \quad (\text{A3})$$

$$F_{x_3} = m_3 \left( -\omega^2 x_3 + \frac{g(x_3 - x_2)}{l_3} \right), \quad (\text{A4})$$

$$M = -I_r \omega^2 \theta + k_r \theta + k_b(x_2 - x_b - \theta l_r) l_r + i \cdot \omega \gamma_\theta^1 \theta, \quad (\text{A5})$$

$$F_{VM_x} = -m_x \omega^2 x + g \left( \frac{m_c(x - x_c)}{l_c} + \frac{m_1(x - ns_x)}{l_1} + \frac{m + m_c + m_1}{l_x} \right), \quad (\text{A6})$$

$$F_{VM_c} = -m_c \left( \frac{g(x - x_c)}{l_c} + \omega^2 x_c \right), \quad (\text{A7})$$

$$F_{VM_1} = -m_1 \left( \frac{g(x - x_1)}{l_1} + \omega^2 x_1 \right) - k_{\text{opt}}(x_2 + x_1 - \theta l_r). \quad (\text{A8})$$

Here  $g$  is the acceleration of gravity and  $\omega$  the angular frequency.  $x_d$  and  $x_3$  are the longitudinal co-ordinates of the pointlike masses of the AX branch, while  $x_2$  and  $\theta$  are the longitudinal and rotational degree of freedom of the

AX mirror.  $x$ ,  $x_c$ , and  $x_1$  are the longitudinal coordinates of the masses of the VM side. The seismic noise sources are included in the model by means of the terms  $ns_d$  and  $ns_x$  which appear in the Eqs. (A1) and (A5). Finally  $I_r$  is the momentum of inertia of the AX mirror,  $k_r$  its torsional coupling constant, and  $l_r = 4$  mm is the distance between the AX mirror center and the point where the light beam hits the mirror. The dissipation factors  $\gamma_l = \gamma_l^1/m_2$  and  $\gamma_\theta = \gamma_\theta^1/I_r$  have been already defined in the previous section, while values of the masses and wire lengths are reported in Table II. The feedback effect

$$F_{fb} = 4 \frac{\alpha}{Z(\omega)} [(x_1 + \theta l_r - x_2 + n_1) G_{\text{opt}} F_{\text{DSP}} + n_2], \quad (\text{A9})$$

where  $n_1$  and  $n_2$  are the ADC and DAC + driver noise

sources.  $Z = j\omega L + R$  is the actuator impedance ( $L = 7 \times 10^{-4}$  H and  $R = 110 \Omega$ ),  $G_{\text{opt}}$  is the optical gain (see Table III) and  $F_{\text{DSP}}$  is the filter transfer function computed by the DSP.  $F_{\text{DSP}}$  is obtained as the sum of two functions; the first one includes a pole at  $\nu_p = 0.5$  Hz increasing the gain at low frequency, and the second one includes a zero at 30 Hz stabilizing the loop. The explicit expression of this function is

$$F_{\text{DSP}} = \frac{-(b_1 + b_2 \cdot i) \cdot (-a_1 + a_2 \cdot i + \nu) \cdot (a_1 + a_3 \cdot i + \nu)}{\pi \nu_p - 2\pi \nu \cdot i}, \quad (\text{A10})$$

where  $b_1 = 0.003$  s,  $b_2 = 0.075$  s,  $a_1 = 13.83$  Hz,  $a_2 = 51.92$  Hz, and  $a_3 = 21.42$  Hz.

- 
- [1] J. K. Thorne and B. Shutz, *Classical Quantum Gravity* **16**, A131 (1999).
- [2] G. Ballardin *et al.*, *Rev. Sci. Instrum.* **72**, 3643 (2001).
- [3] S. Braccini *et al.*, *Astropart. Phys.* **23**, 557 (2005).
- [4] R. Kubo, *Rep. Prog. Phys.* **29**, 255 (1966).
- [5] H. B. Callen and T. A. Welton, *Phys. Rev.* **83**, 34 (1951).
- [6] P. Saulson, *Phys. Rev. D* **42**, 2437 (1990).
- [7] M. Gonzales and P. Saulson, *J. Acoust. Soc. Am.* **96**, 207 (1994).
- [8] K. Yamamoto *et al.*, *Classical Quantum Gravity* **19**, 1689 (2002).
- [9] Courty *et al.*, *Phys. Rev. Lett.* **90**, 083601 (2003).
- [10] Numata *et al.*, *Phys. Rev. Lett.* **91**, 260602 (2003).
- [11] M. Ohashi *et al.*, *Classical Quantum Gravity* **20**, S599 (2003).
- [12] A. Di Virgilio *et al.*, *J. Phys.: Conf. Ser.* **32**, 346 (2006).
- [13] A. Di Vigilio *et al.*, *Phys. Rev. A* **74**, 013813 (2006).
- [14] M. Evans (Virgo Collaboration), "Virgo Status," Moriond07 GW and experimental gravity, LaThuile, 2007, edited by J. Dumarchez (to be published).
- [15] G. Losurdo *et al.*, *Rev. Sci. Instrum.* **72**, 3654 (2001).
- [16] M. Bernardini, E. Majorana, P. Puppò, P. Rapagnani, F. Ricci, and G. Testi, *Rev. Sci. Instrum.* **70**, 3463 (1999).
- [17] VIRGO Collaboration, *VIRGO Physics Book, Optics and related Topics*, Chap. II. Can be downloaded from <http://www.VIRGO.infn.it/>.
- [18] R. C. Ritter and G. T. Gillies, *Phys. Rev. A* **31**, 995 (1985).
- [19] N. A. Robertson *et al.*, *Classical Quantum Gravity* **19**, 4043 (2002).
- [20] Cagnoli *et al.*, *Phys. Lett. A* **213**, 245 (1996).
- [21] G. Cagnoli *et al.*, *Phys. Lett. A* **255**, 230 (1999).
- [22] A. Di Virgilio, VIRGO Note, Report No. VIR-NOT-PIS-1390-334.
- [23] S. M. Kay, *Fundamentals of Statistical Signal Processing*, Prentice Hall Signal Processing Vol. I, edited by Alan V. Hoppenheim (Prentice Hall, Englewood Cliffs, NJ, 1993).
- [24] <http://www.icrr.u-tokyo.ac.jp/gr/gre.html>.
- [25] M. Ohashi *et al.*, *Classical Quantum Gravity* **24**, 2415 (2007) (GWDAW11 proc.)
- [26] M. Ohashi (private communication).
- [27] M. Punturo, VIRGO Note VIR-NOT-PER-1390-51.